Stereocontrol via Propeller Chirality in FLP-Catalyzed Asymmetric Hydrogenation

B. Kótai,[a,b] G. Laczkó,[a,b] A. Hamza,[a] I. Pápai [a]*

[a] Institute of Organic Chemistry, Research Centre for Natural Sciences, H-1117 Budapest, Magyar tudósok körútja 2, Hungary. E-mail: papai.imre@ttk.hu

[b] Hevesy György Ph.D. School of Chemistry, Eötvös Loránd University, P.O. Box 32, H-1518 Budapest, Hungary

Abstract

Utilization of chiral frustrated Lewis pairs as catalysts in enantioselective hydrogenation of unsaturated molecules represents a promising approach in asymmetric synthesis. In our effort to improve our current understanding of the factors governing the stereoselectivity in these catalytic processes, herein we examined the mechanism of direct hydrogenation of aromatic enamines catalyzed by a binaphthyl-based chiral amino-borane. Our computational analysis reveals that only one particular conformer of the key borohydride reaction intermediate can be regarded as a reactive form of this species. This borohydride conformer has a well-defined chiral propeller shape, which induces facial selectivity in the hydride transfer to pro-chiral iminium intermediates. The propeller chirality of the reactive borohydride conformer is generated by the axially chiral binaphthyl scaffold of the amino-borane catalyst through stabilizing π–π stacking interactions. This new computational insight can be readily used to interpret the high degree of stereoinduction observed for these reactions. We expect that the concept of chirality relay could be further exploited in catalyst design endeavors.

Introduction

The cooperative action of unquenched Lewis acid-base pairs, the so-called frustrated Lewis pairs (FLPs), can induce remarkable bond activation in small molecules, which opens novel strategies in chemical synthesis.[1] The facile and reversible heterolytic cleavage of molecular H_2 by main-group FLPs, for instance, enables the development of metal-free methods for direct catalytic hydrogenation of unsaturated species.[2] Asymmetric hydrogenation has been of particular interest since the formulation of the FLP concept, and remarkable achievements have been reported along these lines.[3]

The utilization of chiral boranes as catalysts is a straightforward perception in controlling the stereoselectivity of hydrogenation processes, and several examples demonstrate the potential of this approach (Chart 1a).[4,5,6] The first precedents reported by Klankermayer et al. (boranes **1** and **2**)[4] established that enantiomerically pure boranes generated via hydroboration of chiral olefins with the Piers' borane $(C_6F_5)_2BH$[7] can induce notable stereoselectivity in the hydrogenation of imines. Following this procedure, binaphthyl-based *bis*-boranes **3** were introduced by Du et al.[5] and some members in this family of chiral boranes were found to be remarkably efficient catalysts in asymmetric hydrogenation of various unsaturated substrates, such as imines,[5a] silyl enol ethers[5b] and heteroarenes.[5c-f] Bicyclic *bis*-boranes **4** and **5** developed recently by Wang et al.[6] represent additional examples for successful catalytic application of chiral boranes. C_2-symmetric boranes **4** were shown to yield uniquely high enantioselectivities in imine hydrogenation,[6a] whereas spiro-bicyclic boranes **5** gave excellent stereoselectivities for the hydrogenation of quinolines[6b] and 2-vinylpyridines.[6c] There have been only a few studies reported so far aiming at the utilization of chiral bases as catalysts for FLP-type asymmetric hydrogenation (Chart 1b). The Stephan group employed chiral phosphines, for example (*S*,*S*)-diop (**6**), as intermolecular FLP components in catalytic imine hydrogenation, but only modest enantioselectivities could be observed.[2b] However, Du and co-workers have recently demonstrated this strategy to be a promising direction.[8] They showed that chiral oxazolines (e.g. **7**) combined with achiral

boranes can induce significant degree of enantioselectivity in asymmetric hydrogenation of aryl-alkyl ketones, 1-tetralone-derived enones, and chromones. The concept of combining chiral bases with achiral Lewis acids has recently been extended to heterogeneous catalysis by incorporating the FLP partners into a metal-organic framework. [9]

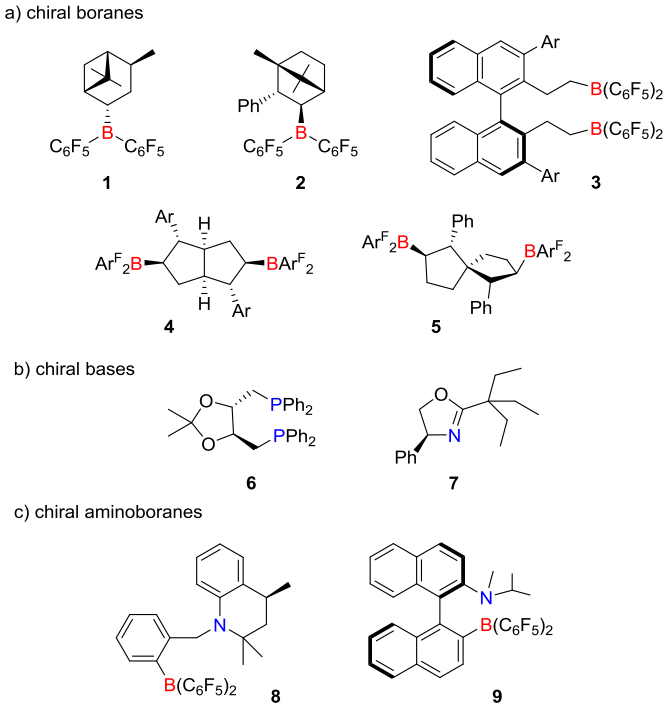

Chart 1. Selection of chiral FLP components employed as catalysts in asymmetric hydrogenations. Ar denotes aromatic substituents; $Ar^F = C_6F_5$ or *p*-C_6F_4H

Attempts to develop chiral intramolecular FLPs for asymmetric catalytic hydrogenation have so far focused on amino-boranes (Chart 1c). FLP **8**, developed by the Repo group, involves a chiral amine unit, and it represents the first example of successful application of this concept.[10] This group later introduced the binaphthyl bridged amino-borane **9**, which was shown to be a powerful hydrogenation catalyst, particularly for asymmetric hydrogenation of enamines. [11]

These results represent important advances in stereo-selective organic synthesis, however, the design of novel chiral FLPs applicable for a wider range of substrates or to improve the catalytic efficiency in asymmetric hydrogenation is challenging. Deeper mechanistic insight and higher level of comprehension regarding the stereoselectivity controlling factors in these catalytic processes may assist catalysis development. Computational approaches have emerged as a valuable tool in elucidating the origin of stereoselectivity in asymmetric catalytic transformations, [12,13] which we think can be exploited in the development of chiral FLP catalysts as well.

In a recent contribution,[14] we have presented a detailed computational analysis for a series of enantioselective imine hydrogenation reactions catalyzed by chiral boranes (e.g. borane **2**). Our results indicated that the stereoselectivity of these reactions is dictated by a thermodynamically unfavoured borohydride isomer, and not by the most stable, experimentally observed form (Scheme 1). In this latter form, the chiral substituent displays steric hindrance for the approaching substrate. In the more reactive borohydride conformer, the phenyl substituent and the two C_6F_5 aromatic rings create a well-defined chiral environment in the hydride transfer enabling stereoinduction via stabilizing aryl−aryl and alkyl−aryl noncovalent interactions. Computations predicted that these specific interactions could be enhanced with additional substitutions, and this finding was confirmed experimentally. One of the proposed new borane variants was demonstrated to provide notably improved enantioselectivities in asymmetric imine hydrogenations.

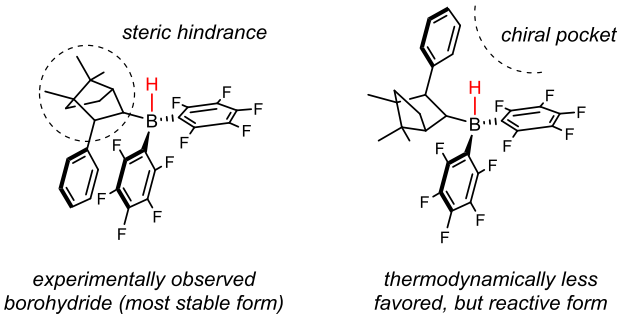

Scheme 1. Two borohydride isomers derived from chiral borane **2.**

These results encourage us to examine the mechanistic details and the source of stereoselectivity of other synthetically important FLP-catalyzed asymmetric hydrogenation processes. In our present work, we scrutinized the origin of stereocontrol in enamine hydrogenation reactions catalyzed by the binaphthyl linked amino-borane **9** (Scheme 2). The reaction with acyclic pyrrolidine derived enamine **en$_1$** gave high enantioselectivity (95% *ee*), and catalyst **9** was shown to be particularly efficient for the hydrogenation of cyclic enamine **en$_2$** (99% *ee*).[11] Our initial DFT calculations carried out for this latter reaction could account for the sense of the observed stereoselectivity, however, the barriers predicted for the formation of the enantiomeric products underestimated the observed enantioselectivity.[15] The computational study highlighted the significance of noncovalent interactions in stereocontrol, but no simple stereoselectivity model could be proposed to interpret the experimental findings.

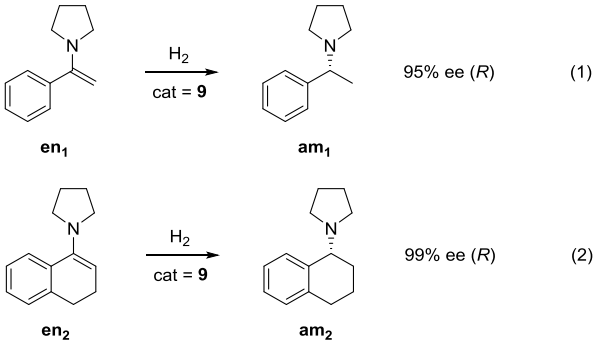

Scheme 2. Reactions examined computationally in this work. H_2 (2 bar), solvent: methyl *tert*-butyl ether, 25 °C, 0.5 h, *ee* determined by HPLC.

Herein, we provide a detailed analysis of the reaction pathways in the catalytic hydrogenation of enamines **en$_1$** and **en$_2$** (Scheme 2). We consider all relevant conformers of the borohydride intermediate formed in the catalytic cycle, and identify the hydride transfer transition states leading to the enantiomeric amine products in these reactions. We demonstrate that only one particular borohydride conformer can be regarded as a reactive form of this intermediate and the enantioselectivity can be readily interpreted by the well-defined shape of this species.

Computational details

The electronic structure of the molecular models used in our computational study was described in terms of density functional theory (DFT) using the dispersion-corrected, range-separated hybrid exchange-correlation functional ωB97X-D.[16] This functional was benchmarked and found to give accurate enantioselectivity predictions for analogous hydrogenation reactions.[14] The geometry optimizations were carried out at the ωB97X-D/6-311G(d,p) level, and for each located structure, we performed vibrational normal mode analysis at the same level. The thermal and entropic contributions to the Gibbs free energies were computed for 298.15 K and c = 1 mol/dm^3 conditions and employing Grimme's *quasi*-RRHO approximation.[17] All located transition states were verified via intrinsic reaction coordinate (IRC) calculations. The solvent effects were estimated by computing the solvation free energies at the

ωB97X-D/6-311G(d,p) level for the optimized structures using the SMD solvation model.[18] Diethyl ether was chosen as a solvent to model the etheric medium used in the hydrogenation experiments.[11] Additional single-point energies were computed for each structure with the larger 6-311++G(3df,3pd) basis set. The energy values reported in the paper refer to solution-phase Gibbs free energies. All DFT calculations were performed using *Gaussian16*.[19] For further computational details, see the Supporting Information (SI).

The conformational space of the molecular species (reaction intermediates and transition states) involved in the investigated reactions was thoroughly explored in our computational study. For simple reaction components, the conformers could be mapped systematically by scanning the DFT potential energy surfaces, but for more complex (bimolecular) reaction intermediates and transition states, the conformational space was initially screened via Monte Carlo sampling. This latter conformational search was carried out by using the OPLS_2005 force field as implemented in the *MacroModel* software.[20] Several conformers were identified via this initial screening, and they were all subject to subsequent DFT calculations. Special attention was given to map all possible conformations for the key transition states of the catalytic cycles. In these cases, the initial conformational search was followed by systematic exploration pertaining the variation of all relevant conformational degrees of freedom (conformational variation of reacting partners, their relative orientation, facial approach of the substrate, etc.). This combined approach in conformational analysis (initial screening plus systematic conformational search) was essential to obtain reliable free energy predictions.

Mechanism of FLP-catalyzed enamine reduction

The FLP-assisted hydrogenation of enamines employing molecular hydrogen[21] is known to take place in three distinct steps as illustrated in Scheme 3.[2c,2e,2j] The first step corresponds to the heterolytic splitting of H_2 by the FLP catalyst **cat**. In principle, H_2 splitting can eventuate in an intermolecular manner involving the borane site of catalyst **9** and the enamine substrate as a base, or even the solvent diethyl ether as a base. However, these mechanistic scenarios can be clearly excluded for two reasons: a) intermolecular H_2 activation with an external base is disfavored entropically, and b) amino-borane **9** cleaves H_2 easily in the absence of the substrate at mild conditions in toluene as well.[11, 22] Following H_2 activation, the hydrogenated catalyst **cat**H_2 first protonates the enamine substrate **en** at the nucleophilic carbon site of the olefinic bond, which yields an iminium intermediate **en**H^+ and an anionic borohydride **cat**H^-. In a subsequent step, the iminium is reduced via hydride transfer from **cat**H^- to give the amine product **am**. The hydride transfer process represents the stereoselectivity determining step of the catalytic cycle, which will be of primary focus in our present work.

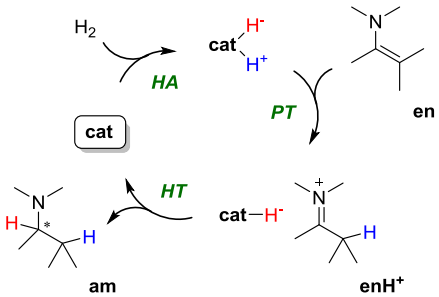

Scheme 3. Mechanistic view of FLP-catalyzed enamine reduction. Notations: **cat**, **en** and **am** denote generic FLP catalyst, enamine and amine molecules; *HA*, *PT* and *HT* refer to hydrogen activation, proton transfer and hydride transfer steps of the reaction, respectively.

As demonstrated previously,[11] catalyst **9** activates H_2 very efficiently (complete conversion within 1 minute at room temperature), which is corroborated by the low free energy barrier ($\Delta G^{\ddagger}$ = 14.8 kcal/mol) and the exergonicity (ΔG = –7.7 kcal/mol) predicted by DFT calculations for this reaction step (for

details, see section 2.1 of the SI). The proton transfer (PT) and hydride transfer (HT) processes involved in the examined reactions will be discussed in detail in our paper, but due to the key importance of the borohydride intermediate (**9**H$^-$) formed upon the protonation step, we first investigate the conformational space of this reaction intermediate.

Conformational space of borohydride 9H$^-$

Four distinct energetically low-lying conformers could be identified for borohydride **9**H$^-$ via conformational analysis, which are depicted in Figure 1.

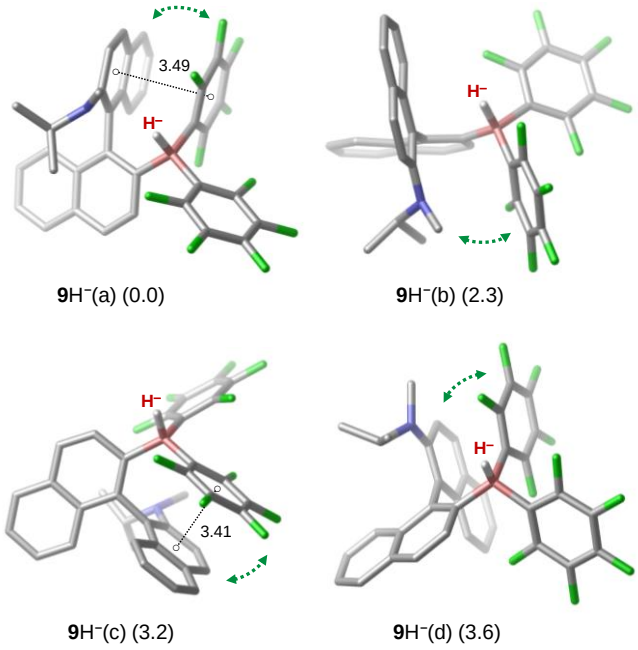

Figure 1. Structures identified computationally for borohydride **9**H$^-$. Relative stabilities are given in parenthesis (in kcal/mol). All C-H hydrogens are omitted for clarity. Intramolecular contacts between the amino-binaphthyl and perfluoro-phenyl groups of the catalyst are highlighted with green arrows. Selected distances between the centers of parallel aryl rings are given in Å.

The most stable form of borohydride **9**H$^-$ (conformer **9**H$^-$(a)) is analogous to the structure of the hydrogenated catalyst **9**H$_2$ (see Figure S2 in the SI), so the B-H unit is positioned in the vicinity of the catalyst's amine group. Stabilizing π–π stacking interactions are apparent in this conformer as illustrated by short distances between the parallel aryl rings. Structure **9**H$^-$(b) can be derived by the rotation around the B-C(binaphthyl) bond, which disables the π–π stacking contact, but it allows CH_3–π interaction between the amine and C_6F_5 groups (see Figure 1). This conformer is computed to be only 2.3 kcal/mol less stable than **9**H$^-$(a). Additional rotations give rise to two other conformers **9**H$^-$(c) and **9**H$^-$(d), also characterized by π–π stacking interactions, but these forms are thermodynamically less favoured; they are predicted to be at 3.2 and 3.6 kcal/mol in free energy.

Transition states (TSs) associated with the conformational changes of borohydride **9**H$^-$ were identified computationally as well, and the obtained free energy profile is presented in Figure 2. The low barriers computed for the rotational transformations suggest a rapid equilibrium between these forms (for details, see section 2.3 of the SI).

We find it interesting to note that borohydride conformers **9**H$^-$(a) and **9**H$^-$(c) can be both derived from the same and the most favoured structure of the catalyst molecule **9** by formal H$^-$ attack of the Lewis acidic borane unit at the two facial sites (Scheme 4; for conformers of **9**, see the SI, section 2.4). This implies that two discrete Lewis acidity attributes (hydride affinities, for instance) can be assigned to the

same FLP molecule.[23] As shown below, the two hydridic forms of catalyst **9** exhibit substantially different reactivities, which affects the overall mechanism of catalytic hydrogenation and therefore the stereoselectivity as well.

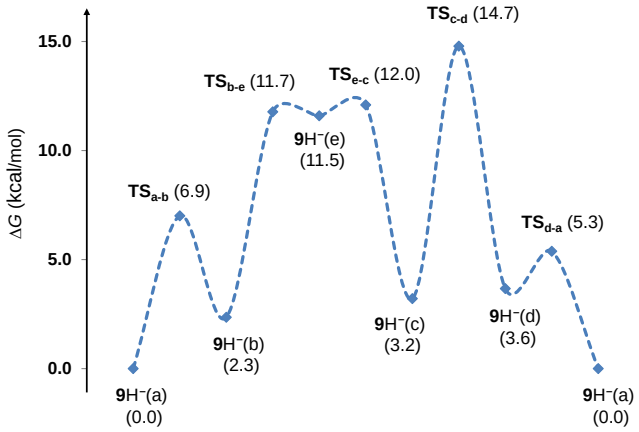

Figure 2. Free energy profile describing the conformational changes in borohydride **9**H⁻. The transition states correspond to rotations of different aryl groups (for details, see section 2.3 of the SI).

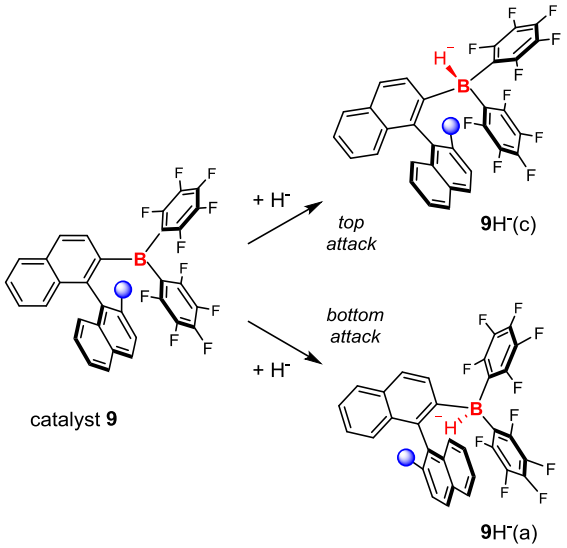

Scheme 4. Multiple Lewis acidity of catalyst **9**. Notation: The amino group on the binaphthyl unit of catalyst **9** is symbolized by blue circle.

Catalytic hydrogenation of enamine $\mathbf{en_1}$

According to the general mechanistic view (Scheme 3), the catalytic cycle of this reaction is initiated with H_2 activation, which is followed by the protonation of substrate $\mathbf{en_1}$. Computations predict the proton transfer to the *Re* face of the enamine slightly more favored over the *Si*-attack (Figure 3; for details, see section 2.5 of the SI). Transition state $\mathbf{TS_{PT\text{-}\mathit{Re}}}$ is at 11.2 kcal/mol in free energy with respect to the reactant state (**9** + $\mathbf{en_1}$ + H_2), which corresponds to a barrier of 18.9 kcal/mol (relative to $\mathbf{9}H_2$ + $\mathbf{en_1}$). This barrier is considerably higher than that of H_2 activation, but it is still easily accessible at room temperature. The product state of the proton transfer via $\mathbf{TS_{PT\text{-}\mathit{Re}}}$ corresponds to a $\mathbf{9}H^-/\mathbf{en_1}H^+$ ion pair intermediate, wherein the borohydride anion adopts **9**H⁻(a) conformation and it is in close contact with the iminium ion (Figure 3). This particular ion pair conformation represents the most stable form of the $\mathbf{9}H^-/\mathbf{en_1}H^+$ intermediate, which is 9.9 kcal/mol below the reactant state. Several other isomeric forms of the $\mathbf{9}H^-/\mathbf{en_1}H^+$ ion pair intermediate were identified computationally and most of them are found to be

within a few kcal/mol in free energy with respect to the most stable form (section 2.6 of the SI). The ensemble of these isomeric forms is expected to be in fast equilibrium, which is ensured by facile dissociation of the **9**H⁻/**en₁**H⁺ ion pair. The dissociated state **9**H⁻ + **en₁**H⁺ of the ion pair intermediate is predicted to be at −2.4 kcal/mol in free energy.

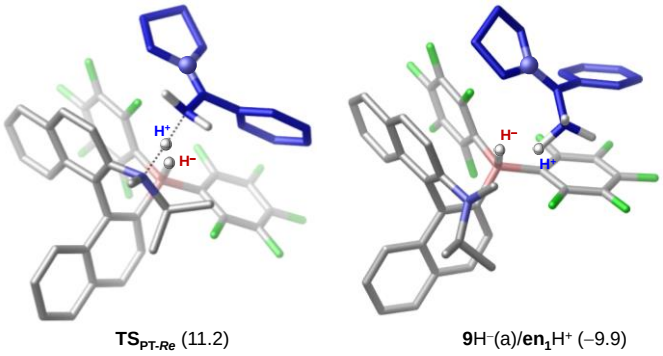

Figure 3. Protonation of the *Re* face of enamine **en₁**. Relative stabilities are given in parenthesis (in kcal/mol, with respect to the **9** + **en₁** + H_2 reactant state). The substrate is highlighted in blue with the N atom in ball representation. Most of the H atoms are omitted for clarity (except for those originating from molecular H_2 and those of the enamine CH_2 group).

A comprehensive conformational analysis was carried out for the HT transition states leading to the enantiomeric (*R*)-**am₁** and (*S*)-**am₁** amine products (for details, see the SI, section 2.7). The most favoured transition states associated with the hydride transfer from the four thermodynamically feasible conformers of the borohydride intermediate **9**H⁻ and delivering the major enantiomeric product (*R*)-**am₁** are shown in Figure 4.

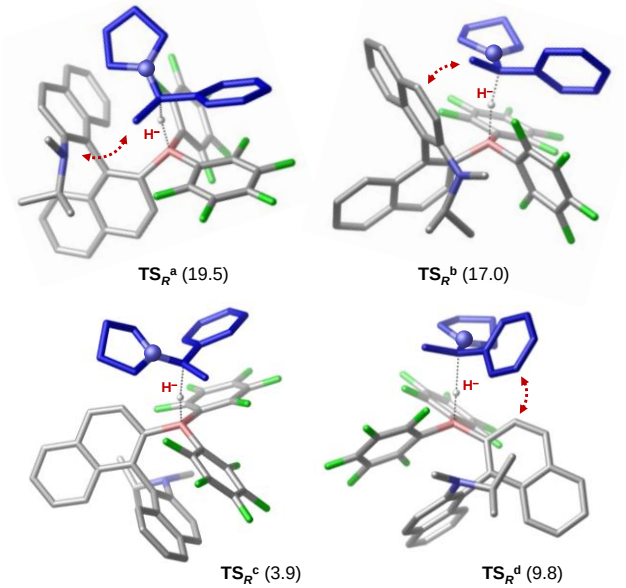

Figure 4. The most favored hydride transfer transition states derived from the four borohydride **9**H⁻ conformers that lead to the (*R*)-**am₁** product. Labels in superscript refer to the borohydride conformer the TS structures correspond to; labels in subscript denote the chirality of the product. Relative stabilities are given in parenthesis (in kcal/mol, with respect to the reactant state). The protonated substrate is highlighted in blue with the N atom in ball representation. Repulsive intermolecular contacts are indicated by red dotted arrows.

Interestingly, transition state **TS$_R^a$** corresponding to hydride transfer from the most stable form of the borohydride (**9**H⁻(a)) is predicted to be the least favoured TS among the four pathways lying 19.5 kcal/mol above the reactants. This TS structure is destabilized due to steric effects imposed by the amino group adjacent to the B-H hydride bond, which hinders the approach of the substrate. Transition state **TS$_R^b$** is found to be slightly more stable, however, steric hindrance is still significant because of the

proximity of the condensed ring of the naphthalene unit in borohydride conformer **9**H⁻(b). The destabilizing steric effects are evidenced by the structural distortions upon the approach of the **en$_1$**H$^+$ cation to the borohydride B-H bond (for structural analysis, see the SI, section 2.8). Repulsive steric intermolecular contacts are minimized in transition state **TS$_R$**$^{\mathbf{c}}$ as the bulky naphthylamine group is positioned on the opposite side of the B-H bond in **9**H⁻(c). Consequently, this TS structure represents the most stable transition state among all explored HT pathways. Finally, the transition state derived from borohydride **9**H⁻(d) (**TS$_R$**$^{\mathbf{d}}$ in Figure 4) is computed to be at 9.8 kcal/mol in free energy implying a certain degree of steric hindrance upon the hydride transfer.

It is remarkable that transition state **TS$_R$**$^{\mathbf{c}}$ is so significantly more favored than those identified on the other HT pathways. This new insight has implication for the mechanistic picture of FLP-assisted hydrogenation of enamines. The free energy profile computed for the entire catalytic cycle in the present hydrogenation reaction suggests that all three elementary steps are exergonic and kinetically allowed (see Figure 5). The results also suggest that the proton transfer is very likely the rate-limiting event. The rapid interconversion in the ensemble of **9**H⁻/**en$_1$**H$^+$ ion pair isomers and a low-barrier HT pathway associated with a specifically reactive form of the borohydride intermediate (**9**H⁻(c)) lead to facile hydride transfer, which however, still represents the stereoselectivity-determining step of the reaction. The computed energetics suggests that the HT process is irreversible (the product state **9** + **am$_1$** is 8.3 kcal/mol below the most favored **9**H⁻/**en$_1$**H$^+$ ion pair, and the barrier of the back transformation is relatively high; 22.1 kcal/mol), so the enantioselectivity of this reaction is under kinetic control.

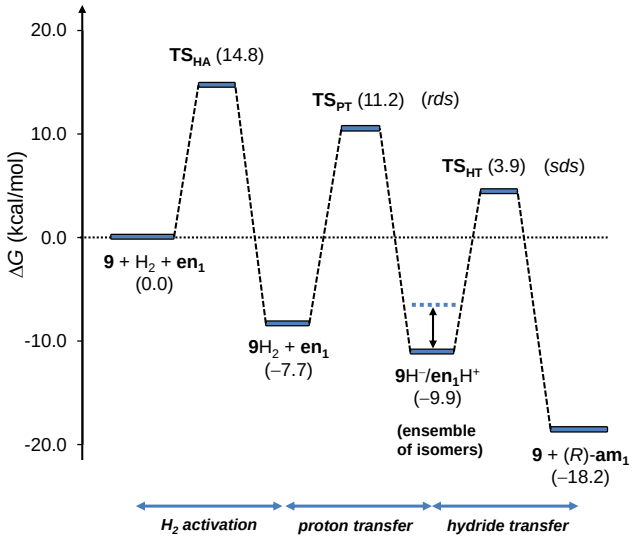

Figure 5. Free energy profile computed for the catalytic cycle in the hydrogenation of **en$_1$**. Energy levels correspond to the most stable forms of intermediates and transition states involved in the reaction. Relative stabilities are given in parenthesis (in kcal/mol, with respect to the reactant state). Labels *"rds"* and *"sds"* refer to rate- and stereoselectivity-determining states of the catalytic cycle. For the general scheme of catalytic cycle, see Scheme 3. The optimized structures of species involved in the reaction are compiled in Figure S15 of the SI.

The relative stabilities computed for the most favored HT transitions states are summarized in the free energy diagram shown in Figure 6. The three lowest lying transition states identified on the competing enantiomeric (*R* and *S)* hydride transfer pathways are all derived from the **9**H⁻(c) borohydride conformer and they differ in the relative orientation of the reaction partners (see section 2.7 of the SI). These transition states are predicted to be within 4 kcal/mol with respect to the most favored **TS$_R$**$^{\mathbf{c}}$. Transition states corresponding to hydride transfer from borohydride **9**H⁻(d) (**TS$_R$**$^{\mathbf{d}}$ and **TS$_S$**$^{\mathbf{d}}$) are found to be considerably less stable, therefore their contribution to the enantioselectivity of hydrogenation is negligible. Transition state **TS$_R$**$^{\mathbf{c}}$ is separated clearly from all other transition states, which can be attributed to stabilizing π–π stacking interactions between the iminium phenyl and the borohydride C_6F_5 substituents (see Figure 6). The most favoured transition state that leads to the formation of the minor

enantiomeric product(*S*)-**am**$_1$ is predicted to be 1.8 kcal/mol less stable giving rise to appreciable enantioselectivity. No intermolecular π-π stacking contacts are present transition state **TS**$_S$^{c}. The enantiomeric excess (*ee*) estimated from the Boltzmann-weighted relative Gibbs free energies of the identified HT transition states is 88.1%, which is in reasonable agreement with the experimental observation (*ee* = 95%).[24]

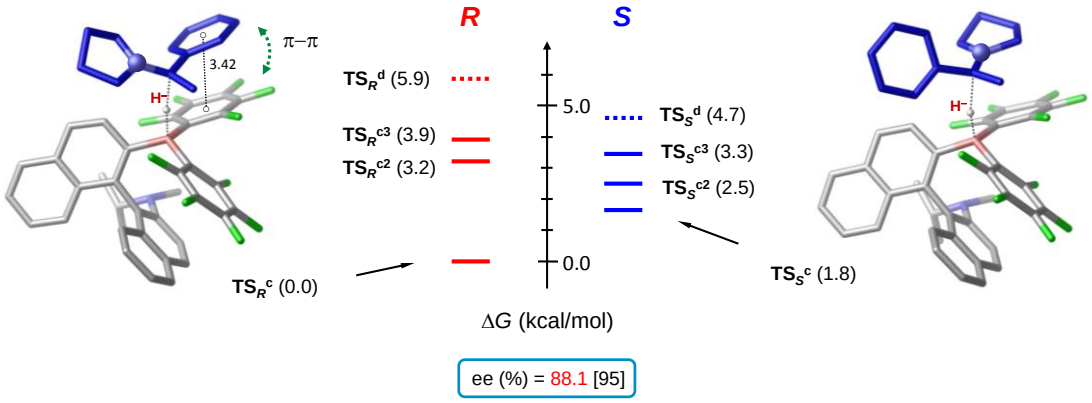

Figure 6. Hydride transfer transition states identified computationally for the hydrogenation of enamine **en**$_1$ with amino-borane catalyst **9**. Each line on the free energy diagram represents a specific transition state isomer with the computed relative stability. **TS**$_R$^{c} and **TS**$_S$^{c} denote the lowest lying transition states leading to the (*R*)-**am**$_1$ and (*S*)-**am**$_1$ products; their relative stabilities are given in parenthesis (in kcal/mol, with respect to the most stable form). Transition states derived from the **9**H$^-$(c) borohydride conformer are represented by solid lines, whereas the dotted lines refer to transition states associated with the **9**H$^-$(d) borohydride form. Stabilizing π–π stacking interactions are highlighted by green dotted arrow. The distance between the centers of selected aryl rings is given in Å. Computed and experimental (in brackets) *ee* data are shown below the diagram.

Catalytic hydrogenation of enamine en$_2$

The hydrogenation of cyclic enamine **en**$_2$ catalyzed by **9** has been previously examined computationally, but the hydride transfer step has only been explored for the two most stable borohydride conformers **9**H$^-$(a) and **9**H$^-$(b).[11] Our present analysis reveals that HT transition states derived from **9**H$^-$(c) are far more favoured in this reaction as well (see section 2.10 of the SI). The free energy profile computed for the energetically most favoured reaction pathway in the catalytic cycle is depicted in Figure 7.

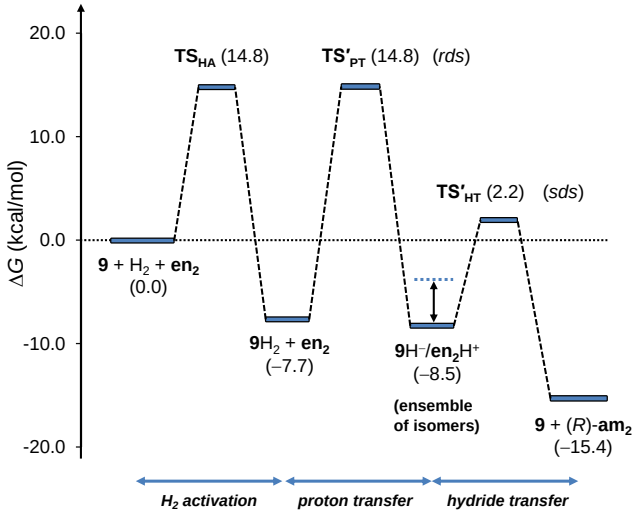

Figure 7. Free energy profile computed for the catalytic cycle in the hydrogenation of **en**$_2$. Energy levels correspond to the most stable forms of intermediates and transition states involved in the reaction. Relative stabilities are given in parenthesis (in kcal/mol, with respect to the reactant state). Labels *"rds"* and *"sds"* refer to rate- and stereoselectivity-determining states of the catalytic cycle. For the general scheme of catalytic cycle, see Scheme 3. The optimized structures of species involved in the reaction are compiled in Figure S17 of the SI.

The protonation of enamine **en₂** is predicted to be less favoured both kinetically and thermodynamically as compared to the analogous process with **en₁**. This is likely due to the fused ring structure of enamine **en₂**, which imposes structural constraint for the pyramidalization of the nucleophilic carbon atom upon the proton transfer (see section 2.12 of the SI), hence the PT transition states are destabilized. The protonation of **en₂** leads to the **9**H⁻/**en₂**H⁺ ion pair intermediate, which forms an ensemble of energetically close-lying isomers that are in fast equilibrium. The most stable form of **9**H⁻/**en₂**H⁺ ion is computed to be at –8.5 kcal/mol on the free energy scale, and the dissociated **9**H⁻ + **en₂**H⁺ state is at –0.7 kcal/mol.

Transition states of the HT step in the hydrogenation of **en₂** have been thoroughly explored and evaluated computationally as well (see section 2.13 of the SI). We found that in analogy to the reaction with the acyclic enamine **en₁**, the transition states associated with the borohydride conformer **9**H⁻(c) are the most favoured TS structures, and they are clearly separated from those derived from the other borohydride forms. The most stable hydride transfer TS (denoted as **TS′$_{HT}$** in Figure 7) yields the major enantiomeric amine product (*R*)-**am₂** and it is predicted to be at 2.2 kcal/mol in free energy. It thus appears that the barrier of the HT step (10.7 kcal/mol) is considerably lower in this reaction as compared to that with **en₁**, which again can be attributed to the structurally constrained bicyclic iminium intermediate **en₂**H⁺ (see section 2.14 of the SI). The barrier of back transformation from the **9** + (*R*)-**am₂** product state to **9**H⁻/**en₂**H⁺ becomes also lower in this reaction (17.6 kcal/mol vs. 22.1 kcal/mol in the reaction with **en₁**), which raises the possibility of racemization upon the reaction course. We note, however, that the catalyst **9** released in the HT step will preferentially react with an H_2 molecule, which is in excess under reaction conditions (2 bar H_2 pressure),[11] so the racemization is not expected (and it was not observed) in this reaction either.[25]

The free energy diagram compiling the computed relative stability data of the most favoured HT transition states along the two enantiomeric pathways in the catalytic hydrogenation of **en₂** is presented in Figure 8.

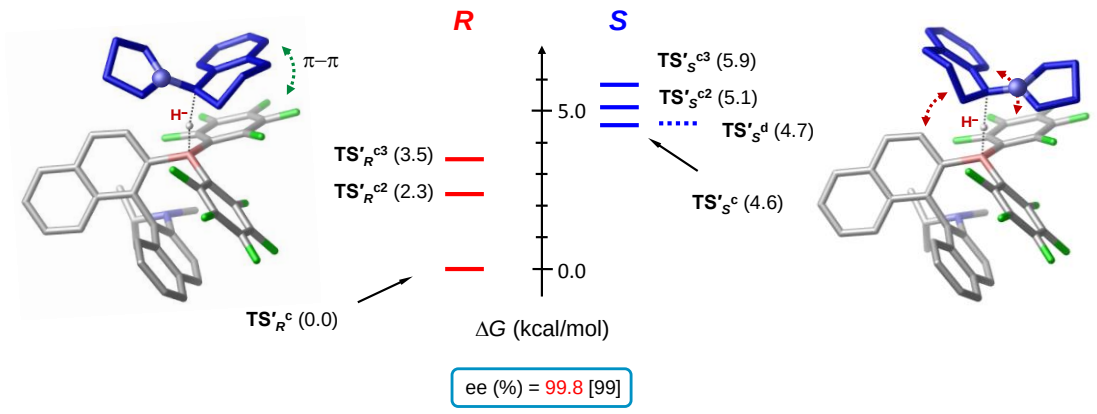

Figure 8. Hydride transfer transition states identified computationally for the hydrogenation of enamine **en₂** with amino-borane catalyst **9**. Each line on the free energy diagram represents a specific transition state isomer with the computed relative stability. **TS′$_R^c$** and **TS′$_S^c$** denote the lowest lying transition states leading to the (*R*)-**am₂** and (*S*)-**am₂** products; their relative stabilities are given in parenthesis (in kcal/mol, with respect to the most stable form). Transition states derived from the **9**H⁻(c) borohydride conformer are represented by solid lines; the dotted line refers to a transition state associated with the **9**H⁻(d) borohydride form. Stabilizing π–π stacking interactions are highlighted by green dotted arrow; red dotted arrows indicate repulsive intermolecular contacts. Computed and experimental (in brackets) *ee* data are shown below the diagram.

It is apparent that all TS structures that yield the minor (*S*)-**am₂** product lie significantly higher in free energy with respect to the most stable **TS′$_R^c$** transition state, producing the major product. The free energy separation is at least 4.6 kcal/mol implying an enhanced enantioselectivity as compared to the reaction with **en₁**. The destabilization of the (*S*)-type transition states is related to the presence of the

fused ring structure of enamine **en$_2$**, which confines the approach of the borohydride even with its sterically most accessible **9**H$^-$(c) form. The degree of destabilization of these forms of TSs is so important that one of the transition states derived from the **9**H$^-$(d) borohydride (**TS′$_S$^{d}** in Figure 8) becomes one of the most stable HT TS structures that give the (*S*)-**am$_2$** product.[26] Based on the computed free energy data, the *ee* of this reaction is estimated to be 99.8%, which is in line with the experimental observation (*ee* = 99%).[11]

Origin of stereocontrol

Our computational analysis suggests that the stereoselectivity of the examined catalytic enamine hydrogenation processes is governed by a thermodynamically less favoured borohydride intermediate, similarly to the asymmetric hydrogenation of imines catalyzed by camphor derived boranes.[14] This feature of the catalytic cycle shows close analogy to the Halpern mechanism of Rh catalyzed asymmetric hydrogenation of activated double bonds.[27] The outstanding reactivity of borohydride conformer **9**H$^-$(c) is clearly related to the lack of steric congestion around the BH unit of this form of the borohydride intermediate. As illustrated by the topographic steric maps computed for the four low-lying borohydride isomers (Figure 9),[28, 29] **9**H$^-$(c) represents the only rotameric state wherein the borohydride B-H bond is not shielded by some parts of the amino-binaphthyl group, so it is easily accessible by the approaching iminium ion. The percent buried volume in a sphere around the hydride center is another descriptor that characterizes the steric congestion, and the computed values support that **9**H$^-$(c) is the least shielded form of the borohydride anion (see %V$_{bur}$ data in Figure 9).

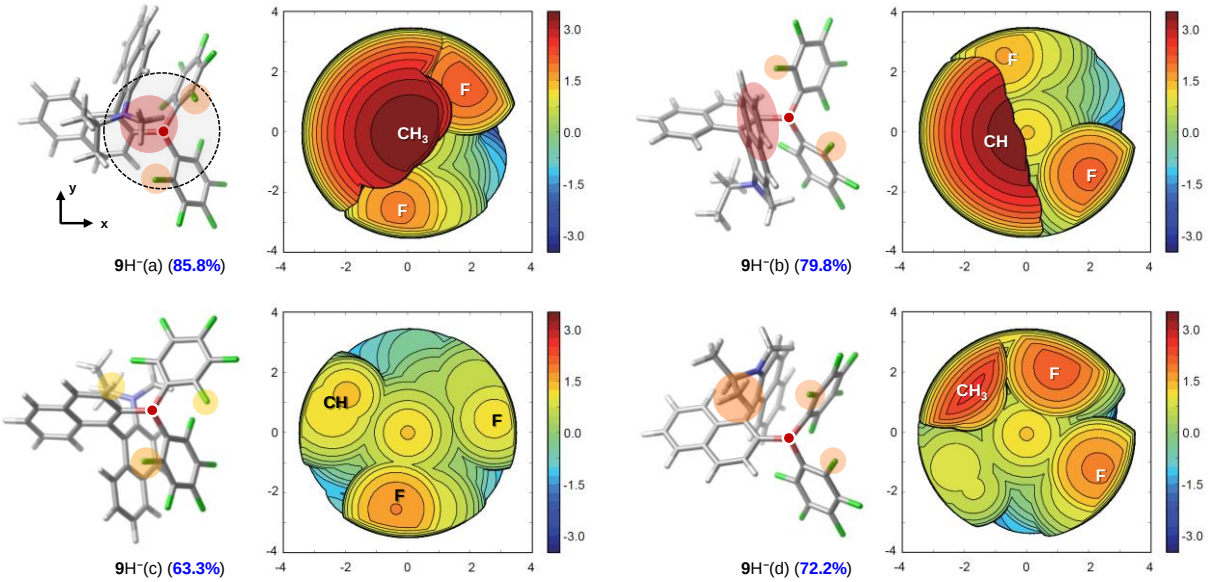

Figure 9. Topographic steric maps of **9**H$^-$ borohydride conformers using DFT-optimized structures. The steric maps are viewed down the z-axis, which is aligned with the B-H bond. The xz-plane is defined by the B-H bond and the adjacent C atom of the binaphthyl group. The origin of the coordinate system corresponds to the hydridic H atom of the borohydride. The 3D maps are defined by the spheres associated with each atom. The scale on the axes and on the isocontour scheme is in Å. The coloring scheme is used to display sterically encumbered regions around the hydride center. The dark red color represents the sterically most hindered regions above the hydride center. The percent buried volume %V$_{bur}$ (displayed in blue) measures the fraction of the space occupied by the atoms in the sphere around the hydride center with radius 3.5 Å. The colored circles displayed on the molecular images highlight the atoms and groups that represent steric hindrance.

The **9**H$^-$(c) form of the borohydride intermediate has a propeller frame with fixed orientation of the three aryl groups that are attached to the boron atom.[30] The propeller chirality of the borohydride is

generated by the axially chiral binaphthyl scaffold of the amino-borane catalyst (Scheme 5) via stabilizing π–π stacking contacts between the back-side naphthyl ring and one of the C_6F_5 groups.

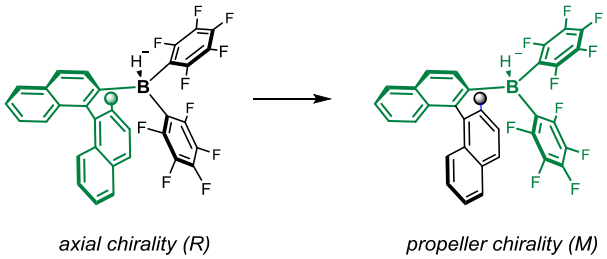

Scheme 5. Chirality transfer in borohydride **9**H⁻(c).

The chiral propeller framework in **9**H⁻(c) enables facial discrimination in the hydride transfer to aryl iminium ions $\mathbf{en_1}H^+$ and $\mathbf{en_2}H^+$ because stabilizing π–π stacking interactions can develop upon the attack of the *Re*-face of the iminiums, leading to the formation of the (*R*) amine products. These interactions are apparent on the NCI plots generated for transition states $\mathbf{TS}_R{}^c$ and $\mathbf{TS'}_R{}^c$ (see Figure 10).[31] For transition states supplying the (*S*) products, no such π–π stacking interactions are identified, but instead, some of the contacts become repulsive and destabilize the $\mathbf{TS}_S{}^c$ and $\mathbf{TS'}_S{}^c$ transition states. Destabilizing steric effects are more significant for the bulkier and structurally more constrained cyclic enamine $\mathbf{en_2}$, leading to increased enantioselectivity with this substrate.

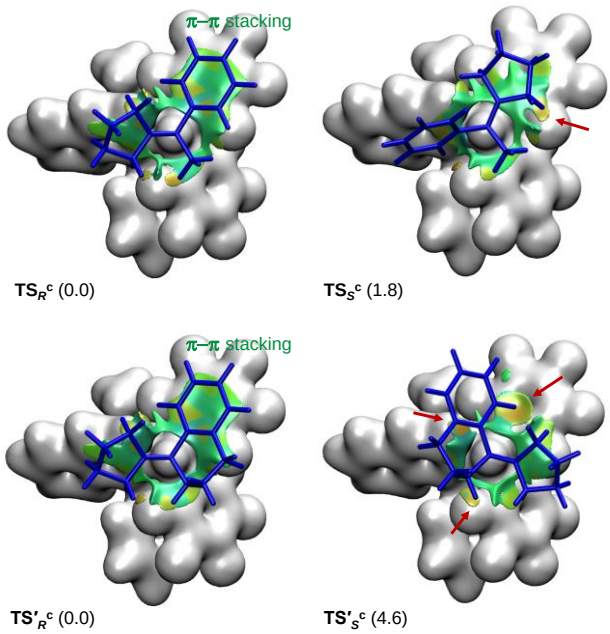

Figure 10. Noncovalent interactions (NCI) in HT transition states that primarily determine the enantioselectivity of catalytic hydrogenations of $\mathbf{en_1}$ ($\mathbf{TS}_R{}^c$ and $\mathbf{TS}_S{}^c$) and $\mathbf{en_2}$ ($\mathbf{TS'}_R{}^c$ and $\mathbf{TS'}_S{}^c$). Borohydride **9**H⁻(c) is represented by a gray isodensity surface (ρ= 0.02 au); the iminium species are shown in blue. The applied cutoff for reduced density gradient is s = 0.3 au. Orange surface areas designate destabilizing steric interactions and some of them are highlighted by red arrows as well. Relative stabilities of TS structures are given in parentheses (in kcal/mol).

It is also worth mentioning that the second least shielded borohydride isomer **9**H⁻(d) has a propeller shape as well (see Figure 1), however, the orientation of the three aryl groups is reversed as compared to that in **9**H⁻(c). The reversed propeller chirality of **9**H⁻(d) enables π–π stacking contacts only in transition states leading to the minor (*S*) products ($\mathbf{TS}_S{}^d$ and $\mathbf{TS'}_S{}^d$), therefore, these transition states will be more favoured than the corresponding $\mathbf{TS}_R{}^d$ and $\mathbf{TS'}_R{}^d$ TS structures (see Figures 6 and 8). This observation supports the significance of stabilizing π–π stacking interactions in stereocontrol.

On the role of binaphthyl framework

Sterically congested binaphthyl frameworks have been widely used as chiral building blocks in catalysts employed in enantioselective synthesis. For instance, BINOL-derived Brønsted acids are among the most efficient organocatalysts,[32] whereas BINAP type compounds are considered as the most important ligands in transition metal asymmetric catalysis (see Chart 2).[33] The C_2-symmetric binaphthyl backbone does not involve stereogenic atomic centers, but the locked orientation of the two naphthyl groups creates an asymmetric environment for substrate activation, which can be further tuned by additional bulky substituents at the 3,3′ positions. Related computational studies identified steric effects as key factors that control the stereoselectivity of these organocatalytic and transition metal catalyzed asymmetric transformations.[34]

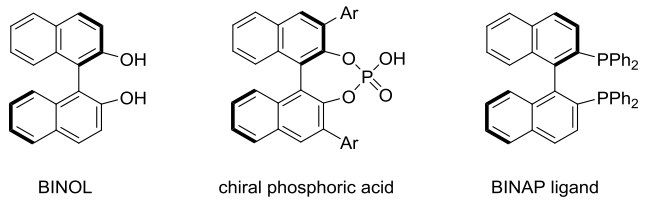

Chart 2. Privileged binaphthyl frameworks in asymmetric catalysis.

In the asymmetric hydrogenation reactions examined herein, the binaphthyl framework of catalyst **9** represents a bulky aryl substituent at the Lewis acidic boron center. However, this axially chiral unit does not participate directly in stereocontrol via steric effects, it actually hinders the approach of the substrate in the stereoselectivity determining hydride transfer step, but it assists the formation of a reactive intermediate with a well-defined chiral propeller shape. Consequently, the atropoisomeric chirality of the binaphthyl framework is transferred to propeller chirality, which is an essential stereocontrol element in the present catalytic enamine hydrogenation process.[35]

Chirality transfer from the axially chiral binaphthyl framework to propeller-shaped chirality of triaryl boranes has been previously recognized for a binaphthyl based amino-borane analogous to **9**.[36] Introducing dimethylamino (NMe_2) and dimesitylboryl ($BMes_2$) groups at the 2,2′-positions of the binaphthyl framework, Zhao et al. achieved propeller chirality at the boron center. The chirality relay was associated with intramolecular π–π stacking contacts, which could be confirmed experimentally via X-ray and NMR measurements. The influence of the propeller chirality of the boron center on the chiroptical properties has also been examined, but it could not be clearly detected.[37] Herein we demonstrated that the chirality relay manifested in the borohydride state of amino-borane **9** has a crucial role that determines the stereochemical outcome of catalytic enamine hydrogenation.

Finally, we note that in binaphthyl-based *bis*-borane **3** developed by Du et al. (Chart 1), the binaphthyl unit is not directly linked to the catalytically active boron center, so the three-blade propeller shape cannot be established in the corresponding borohydride state. However, stabilizing aryl-aryl contacts between the aryl-decorated binaphthyl core and the borane's perfluoro-phenyl substituents may still fix the orientation of the C_6F_5 rings in the borohydride state, providing an asymmetric cavity for the substrate. Our preliminary study carried out for the hydridic states of borane **3** supports this view (for results, see section 2.16 of the SI), but more detailed computational studies are needed to fully uncover the origin of stereoinduction in hydrogenation reactions catalyzed by this binaphthyl-based borane.

Conclusions

In this computational study, we aimed at rationalizing the high enantioselectivity observed in the hydrogenation of aromatic enamines $\mathbf{en_1}$ and $\mathbf{en_2}$ catalyzed by the chiral binaphthyl linked amino-borane **9**.[11] To this end, we examined all elementary steps of the catalytic cycles, which involve the H_2 activation via the catalyst, the rate-limiting protonation of the enamine substrate, and the subsequent stereoselectivity determining hydride transfer step.

We found that the borohydride intermediate formed upon protonation has several energetically close-lying conformers, which are in fast equilibrium. The comprehensive exploration of various hydride transfer reaction pathways indicated that one of the borohydride conformers, albeit not the most stable one, is significantly more reactive than the other isomeric forms. The enhanced reactivity of this conformer stems from the unshielded B-H bond, which becomes more accessible by the iminium intermediate leading to notably reduced hydride transfer barrier. We showed that the stereoselectivity of enamine hydrogenation is essentially governed by this particular borohydride form. The transition states identified along the hydride transfer pathways leading to the two enantiomeric products could well account for the observed enantioselectivities.

The new mechanistic insights allowed us to formulate a simple stereoselectivity model for the investigated asymmetric hydrogenation reactions. In the most reactive form of the borohydride intermediate, the three aryl groups at the boron center constitute a propeller structure. The orientation of the aryl groups is determined by the axial chirality of the binaphthyl scaffold. The chirality transfer in this borohydride species is enabled by π–π stacking contacts. The chiral propeller-shaped triaryl framework induces facial selectivity in the hydride transfer to prochiral iminiums. The role of stabilizing π–π stacking interactions in stereoinduction could be clearly demonstrated computationally. Steric properties of the enamine substrate were shown to be important as well. The bulkier and structurally more constrained cyclic enamine **en$_2$** encounters increased steric hindrance on the minor reaction pathway, which enhances the stereoselectivity.

Asymmetric hydrogenation catalyzed by chiral frustrated Lewis pairs is a promising and growing research field. One common strategy in catalyst development is to implement stereogenic centers in close vicinity of the reactive Lewis acidic sites. Alternatively, axially chiral units, such as the binaphtyl framework, can be successfully utilized as a chiral building block. In our present work, we provided new computational insight into the origin of stereocontrol for the latter class of reactions, which we think could be exploited in future synthetic developments.

Acknowledgements

Financial support from the National Research, Development, and Innovation Office (NKFIH) is gratefully acknowledged (grant K-142486).

Notes and references

[1] For reviews on FLP chemistry, see: (a) G. Erker and D. W. Stephan, Topics in Current Chemistry, Eds. Springer-Verlag, 2013, Vols. 332 and 334; (b) D. W. Stephan and G. Erker, *Angew. Chem., Int. Ed.*, 2015, **54**, 6400; (c) D. W. Stephan, *J. Am. Chem. Soc.*, 2015, **137**, 10018; (d) D. W. Stephan, Acc. Chem. Res. 2014, **48**, 306; (e) D. W. Stephan, *Science*, 2016, **354**, aaf7229; (f) A. R. Jupp and D. W. Stephan, *Trends in Chemistry*, 2019, **1**, 35; (g) J. C. Slootweg and A. R. Jupp, Frustrated Lewis Pairs, Molecular Catalysis 2, Eds.; Springer Nature, Switzerland, AG, 2020; (h) K. Stefkova, J. L. Carden and R. L. Melen, Chemistry, *Molecular Sciences and Chemical Engineering*, Elsevier Reference Collection, Elsevier, 2021. i) J. Paradies, *Acc. Chem. Res.*, 2023, **56**, 7, 821.

[2] For reviews on FLP-type catalytic hydrogenations, see: (a) D. W. Stephan and G. Erker, *Angew. Chem., Int. Ed.*, 2010, **49**, 46; (b) D. W. Stephan, S. Greenberg, T. W. Graham, P. Chase, J. J. Hastie, S. J. Geier, J. M. Farrell, C. C. Brown, Z. M. Heiden, G. C. Welch and M. Ullrich, *Inorg. Chem.*, 2011, **50**, 12338; (c) D. W. Stephan and G. Erker, *Topics in Current Chemistry*, Springer, Berlin, Heidelberg 2013, **332**, 85; (d) V. Sumerin, K. Chernichenko, F. Schulz, M. Leskelä, B. Rieger and T. Repo, *Topics in Current Chemistry*, Springer, Berlin, Heidelberg 2013, **332**, 111; (e) J. Paradies, *Angew. Chem., Int. Ed.*, 2014, **53**, 3552; (f) L. J. Hounjet and D. W. Stephan, *Org. Process Res. Dev.*, 2014, **18**, 385; (g) D. J. Scott, M. J. Fuchter and A. E. Ashley, *Chem. Soc. Rev.*, 2017, **46**, 5689; (h) J. Paradies, *Coord. Chem. Rev.*, 2019, **380**, 170; (i) J. Lam, K. M. Szkop, E. Mosaferi and D. W. Stephan, *Chem. Soc. Rev.*, 2019, **48**, 3592; (j) J. Paradies, *Eur. J. Org. Chem.*, 2019, 283; (k) D. W. Stephan, *J. Am. Chem.*

Soc., 2021, **143**, 20002; (l) D. W. Stephan, A Primer in Frustrated Lewis Pair Hydrogenation: Concepts to Applications, RSC eTextbook Collection, CPI Grou; (UK) Ltd, Croydon, 2021; (m) R. Zhou, Z. P. Tavandashti and J. Paradies, *SynOpen*, 2023, **7**, 46.

[3] For review works, see: (a) D. Chen and J. Klankermayer, *Top. Curr. Chem.*, 2013, **334**, 1; (b) X. Feng and H. Du, *Tetrahedron Lett.*, 2014, **55**, 6959; (c) L. Shi, Y.-G. Zhou, *ChemCatChem*, 2014, **7**, 54; (d) J. Paradies, *Top. Organomet. Chemistry*, Springer International Publishing 2018, **193**; (e) W. Meng, X. Feng and H. Du, *Acc. Chem. Res.*, 2018, **51**, 191; (f) W. Meng, X. Feng and H. Du, *Chinese J. Chem.*, 2020, **38**, 625; (g) X. Feng, W. Meng and H. Du, *Frustrated Lewis Pairs, Molecular Catalysis*, 2, J. C. Slootweg, A. R. Jupp, Eds.; Springer Nature, Switzerland, AG, 2020, 29; h) M. G. Guerzoni, A. Dasgupta, E. Richards and R. L. Melen, *Chem Catal*., 2022, **2**, 2865.

[4] (a) D. Chen and J. Klankermayer, *Chem. Commun.*, 2008, 2130; (b) D. Chen, Y. Wang and J. Klankermayer, *Angew. Chem., Int. Ed.*, 2010, **49**, 9475; (c) G. Ghattas, D. Chen, F. Pan and J. Klankermayer, *Dalton Trans.*, 2012, **41**, 9026.

[5] (a) Y. Liu and H. Du, *J. Am. Chem. Soc.*, 2013, **135**, 6810; (b) S. Wei and H. Du, *J. Am. Chem. Soc.*, 2014, **136**, 12261; (c) Z. Zhang and H. Du, *Org. Lett.*, 2015, **17**, 2816; (d) Z. Zhang and H. Du, *Org. Lett.*, 2015, **17**, 6266; (e) Z. Zhang and H. Du, *Angew. Chem., Int. Ed.*, 2015, **54**, 623; (f) S. Wei, X. Feng and H. Du, *Org. Biomol. Chem.*, 2016, **14**, 8026.

[6] (a) X. Tu, N. Zeng, R. Li, Y. Zhao, D. Xie, Q. Peng and X. Wang, *Angew. Chem., Int. Ed.*, 2018, **57**, 15096; (b) X. Li, J. Tian, N. Liu, X. Tu, N. Zeng and X. Wang, *Angew. Chem., Int. Ed.*, 2019, **58**, 4664; (c) J. Tian, Z. Yang, X. Liang, N. Liu, C. Hu, X. Tu, X. Li and X. Wang, *Angew. Chem., Int. Ed.*, 2020, **59**, 18452.

[7] (a) D. J. Parks, von H. R. E. Spence and W. E. Piers, *Angew. Chem., Int. Ed.*, 1995, **34**, 809; (b) D. J. Parks, W. E. Piers and G. P. Yap, *Organometallics*, 1998, **17**, 5492; (c) E. A. Patrick and W. E. Piers, *Chem. Commun.*, 2020, **56**, 841.

[8] (a) B. Gao, X. Feng, W. Meng and H. Du, *Angew. Chem., Int. Ed.*, 2020, **59**, 4498; (b) Y. Dai, W. Meng, X. Feng and H. Du, *Chem. Commun.*, 2022, **58**, 1558.

[9] Y. Zhang, S. Chen, Al-A. M. Enizi, A. Nafady, Z. Tang and S. Ma, *Angew. Chem., Int. Ed.*, 2023, **62**, e202213399.

[10] V. Sumerin, K. Chernichenko, M. Nieger, M. Leskelä, B. Rieger and T. Repo, *Adv. Synth. Catal.*, 2011, **353**, 2093.

[11] M. Lindqvist, K. Borre, K. Axenov, B. Kótai, M. Nieger, M. Leskela, I. Pápai and T. Repo, *J. Am. Chem. Soc.*, 2015, **137**, 4038.

[12] For a review on experimental and computational mechanistic studies in homogeneous asymmetric catalysis, see: I. D. Gridnev and P. A. Dub, Enantioselection in Asymmetric Catalysis; CRC Press: Taylor & Francis Group, 2017.

[13] For reviews on concepts and challenges in computing stereoselectivities, see: (a) K. H. Hopmann, *Int. J. Quantum Chem.*, 2015, **115**, 1232; (b) Q. Peng, F. Duarte and R. S. Paton, *Chem. Soc. Rev.*, 2016, **45**, 6093; (c) E. H. Krenske, *Applied Theoretical Organic Chemistry*, Ed. D. J. Tantillo, World Scientific: New Jersey, 2018, 583; (d) S. Singh and R. B. Sunoj, *Advances in Physical Organic Chemistry*, 2019, **53**, 1; (e) J. N. Harvey, F. Himo, F. Maseras and L. Perrin, *ACS Catal.*, 2019, **9**, 6803; (f) X. Sheng, M. Kazemi, F. Planas and F. Himo, *ACS Catal*., 2020, **10**, 6430; (f) N. Melnyk, I. Iribarren, E. Mates-Torres, C. Trujillo, *Chem. Eur. J*., 2022, **28**, e202201570.

[14] A. Hamza, K. Sorochkina, B. Kótai, K. Chernichenko, D. Berta, M. Bolte, M. Nieger, T. Repo and I. Pápai, *ACS Catal.*, 2020, **10**, 14290.

[15] For the hydrogenation of **en$_2$**, computations predicted the formation of the major (*R*) product to be kinetically favored by 1.4 kcal/mol, which corresponds to 83% *ee*. The observed *ee* is 99% (see Ref. 11).

[16] (a) J.-D. Chai and Head-M. Gordon, *Phys. Chem. Chem. Phys.*, 2008, **10**, 6615; (b) J.-D. Chai, and Head-M. Gordon, *J. Chem. Phys.*, 2008, **128**, 084106; (c) S. Grimme, *J. Comput. Chem.*, 2006, **27**, 1787.

[17] S. Grimme, *Phys. Chem. Eur. J.*, 2012, **18**, 9955.

[18] A. V. Marenich, C. J. Cramer and D. G. Truhlar, *J. Phys. Chem. B*, 2009, **113**, 6378.

[19] Gaussian 16, Revision A.03, M. J. Frisch, G. W. Trucks, H. B. Schlegel, G. E. Scuseria, M. A. Robb, J. R. Cheeseman, G. Scalmani, V. Barone, G. A. Petersson, H. Nakatsuji, X. Li, M. Caricato, A. V. Marenich, J. Bloino, B. G. Janesko, R. Gomperts, B. Mennucci, H. P. Hratchian, J. V. Ortiz, A. F. Izmaylov, J. L. Sonnenberg, Williams-D. Young, F. Ding, F. Lipparini, F. Egidi, J. Goings, B. Peng, A. Petrone, T. Henderson, D. Ranasinghe, V. G. Zakrzewski, J. Gao, N. Rega, G. Zheng, W. Liang, M. Hada, M. Ehara, K. Toyota, R. Fukuda, J. Hasegawa, M. Ishida, T. Nakajima, Y. Honda, O. Kitao, H. Nakai, T. Vreven, K. Throssell, J. A. Montgomery, , Jr.; J. E. Peralta, F. Ogliaro, M. J. Bearpark, J. J. Heyd, E. N. Brothers, K. N. Kudin, V. N. Staroverov, T. A. Keith, R. Kobayashi, J. Normand, K. Raghavachari, A. P. Rendell, J. C. Burant, S. S. Iyengar, J. Tomasi, M. Cossi, J. M. Millam, M. Klene, C. Adamo, R. Cammi, J. W. Ochterski, R. L. Martin, K. Morokuma, O. Farkas, J. B. Foresman, D. J. Fox, Gaussian, Inc., Wallingford CT, 2016.

[20] Schrödinger Release 2017-1: Schrödinger, LLC, New York, NY, 2017.

[21] For selected examples, see: (a) S. Schwendemann, T. A. Tumay, K. B. Axenov, I. Peuser, G. Kehr, R. Fröhlich and G. Erker, *Organometallics*, 2010, **29**, 1067; (b) P. Spies, S. Schwendemann, S. Lange, G. Kehr, R. Fröhlich and G. Erker, *Angew. Chem. Int. Ed*., 2008, **47**, 7543; (c) J. M. Farrell, J. A. Hatnean and D. W. Stephan, *J. Am. Chem. Soc.*, 2012, **134**, 15728; (d) É. Dorkó, M. Szabó, B. Kótai, I. Pápai, A. Domján and T. Soós, *Angew. Chem., Int. Ed.*, 2017, **56**, 9512.

[22] For experimental and computational studies of FLP assisted hydrogenation reactions, wherein ethereal solvents are known to act as Lewis base partner in H_2 activation, see: (a) T. Mahdi and D. W. Stephan, *J. Am. Chem. Soc.* 2014, **136**, 15809; (b) D. J. Scott, M. J. Fuchter and A. E. Ashley, *J. Am. Chem. Soc.* 2014, **136**, 15813; (c) Á. Gyömöre, M. Bakos, T. Földes, I. Pápai, A. Domján and T. Soós, *ACS Catal*. 2015, **5**, 5366; (d) D. J. Scott, T. R. Simmons, E. J. Lawrence, G. G. Wildgoose, M. J. Fuchter and A. E. Ashley, *ACS Catal.* 2015, **5**, 5540; (e) É. Dorkó, Á. Gyömöre, A. Domján, and T. Soós, *Angew. Chem., Int. Ed.*, 2017, **56**, 5217; (f) Y. Hoshimoto, T. Kinoshita, S. Hazra, M. Ohashi and S. Ogoshi, *J. Am. Chem. Soc.* 2018, **140**, 7292; (g) M. Sultana, A. Paul and L. Roy, *ChemistrySelect* 2020, **5**, 13397.

[23] For the concept of multiple Lewis acidity of triaryl boranes, see: B. Kovács, T. Földes, M. Szabó, É. Dorkó, B. Kótai, G. Laczkó, T. Holczbauer, A. Domján, I. Pápai and T. Soós, preprint, doi: 10.26434/chemrxiv-2024-kj4zz.

[24] The rapid equilibration in the ensemble of $\mathbf{9}H^-/\mathbf{en_1}H^+$ ion pair isomers enables the application of the Curtin−Hammett principle to compute the enantioselectivity via Boltzmann averaging over the Gibbs free energies of the identified HT transition states.

[25] Kinetic simulations carried out for the catalytic hydrogenation of $\mathbf{en_2}$ based on the computed free energy data support the lack of product racemization (for details, see section 2.15 of the SI).

[26] The relative stability of transition state $\mathbf{TS'_R}^{\mathbf{d}}$ derived from borohydride $\mathbf{9}H^-$(d) and leading to the major (*R*)-$\mathbf{am_2}$ product is predicted to be 7.6 kcal/mol, so it is not shown in Figure 8.

[27] J. Halpern, Mechanism and stereoselectivity of asymmetric hydrogenation. *Science*, 1982, **217**, 401.

[28] The topographic steric maps were obtained via the web application at https://www.molnac.unisa.it/OMtools/sambvca2.1/index.html. For related concepts, see: L. Falivene, Z. Cao, A. Petta, L. Serra, A. Poater, R. Oliva, V. Scarano and L. Cavallo, *Nat. Chem*., 2019, **11**, 872.

[29] For a relevant study on the evaluation of steric properties of Lewis acid, see: L. Zapf, M. Riethmann, S. A. Föhrenbacher, M. Finze and U. Radius, *Chem. Sci*. 2023, **14**, 2275.

[30] Triarylboranes themselves are considered as molecular propellers. For fundamental studies regarding the stereochemical consequences of aryl substitutions, see: (a) K. Mislow, *Acc. Chem. Res.*, 1976, **9**, 26; (b) S. Toyota, M. Asakura, M. Oki and F. Toda, *Bull. Chem. Soc. Jpn*., 2000, **73**, 2357; (c) H. Ito, T. Abe and K. Saigo, *Angew. Chem. Int. Ed*., 2011, **50**, 7144.

[31] The NCI analysis was carried out by the NCIPLOT program: (a) E. R. Johnson, S. Keinan, P. Mori-Sánchez, J. Contreras-García, A. J. Cohen and W. Yang, *J. Am. Chem. Soc.*, 2010, **132**, 6498; (b) J. Contreras-García, E. R. Johnson, S. Keinan, R. Chaudret, J.-P. Piquemal, D. N. Beratan and W. Yang, *J. Chem. Theory Comput.*, 2011, **7**, 625.

[32] For selected reviews, see: (a) D. Kampen, C. M. Reisinger and B. List, *Topics in Current Chemistry*, Springer, Berlin, Heidelberg 2010, **291**, 1; (b) D. Parmar, E. Sugiono, S. Raja and M. Rueping, *Chem. Rev.*, 2014, **114**, 9047; (c) M. Hatano and K. Ishihara, *Asian J. Org. Chem*., 2014, **3**, 352; (d) T. Akiyama and K. Mori, *Chem. Rev.*, 2015, **115**, 9277.

[33] For reviews of fundamental works, see: (a) R. Noyori and H. Takaya, *Acc. Chem. Res.*, 1990, **23**, 345; (b) S. Akutagawa, *Appl. Catal. A: Gen*., 1995, **128**, 171.

[34] For related computational studies, see: (a) P. A. Dub, N. J. Henson, R. L. Martin and J. C. Gordon, *J. Am. Chem. Soc.*, 2014, **136**, 3505; (d) P. A. Dub and J. C. Gordon, *Dalton Trans.*, 2016, **45**, 6756; (c) J. P. Reid and J. M. Goodman, *J. Am. Chem. Soc.*, 2016, **138**, 7910; (d) J. P. Reid and J. M. Goodman, *Chem. Eur. J*., 2017, **23**, 14248.

[35] For the concept of chiral relay in asymmetric catalysis, see: O. Corminboeuf, L. Quaranta, P. Renaud, M. Liu, C. P. Jasperse and M. P. Sibi, *Chem. Eur. J.*, 2003, **9**, 28.

[36] C. Wang, Z.-B. Sun, Q.-W. Xu, and C.-H. Zhao, *Chem. Eur. J.*, 2016, **22**, 16750.

[37] For selected works focusing on the chiroptical properties of propeller-shaped triaryl boranes, see: (a) H.-W. Li, M. Li, Z. –H. Zhao, C. –F. Chen, Q. Peng and C. –H. Zhao, *Org. Lett*., 2021, **23**, 4759; (b) M. Kemper, E. Engelage and C. Merten, *Angew. Chem. Int. Ed.*, 2021, 60, 2958; (c) M. Kemper, S. Reese, E. Engelage and C. Merten, *Chem. Eur. J*., 2022, **28**, e202202812